

Fluctuations in EEG band power at subject-specific timescales over minutes to days are associated with changes in seizure dynamics

Mariella Panagiotopoulou¹, Christoforos A Papasavvas¹, Gabrielle M Schroeder¹,
Rhys H Thomas², Peter N Taylor^{1,2,3}, Yujiang Wang^{*1,2,3}

October 17, 2021

1. CNNP Lab (www.cnnp-lab.com), Interdisciplinary Computing and Complex BioSystems Group, School of Computing, Newcastle University, Newcastle upon Tyne, United Kingdom
2. Faculty of Medical Sciences, Newcastle University, Newcastle upon Tyne, United Kingdom
3. UCL Queen Square Institute of Neurology, Queen Square, London, United Kingdom

* Yujiang.Wang@newcastle.ac.uk

Abstract

Epilepsy is recognised as a dynamic disease, where susceptibility to seizures and seizure characteristics change over time. Specifically, we recently found variable seizure dynamics within individual patients. Additionally, the variability appeared to follow subject-specific circadian or longer timescale modulations. However, whether signatures of these modulations over different timescales can be captured on continuous (interictal) EEG remains unclear.

In this work, we analyse continuous interictal intracranial electroencephalographic (iEEG) recordings from video-telemetry units and find fluctuations in iEEG band power over different timescales ranging from minutes up to twelve days.

We find that all subjects show not only an approximately-circadian fluctuation in their EEG band power, but also many other fluctuations on subject-specific timescales. Importantly, we find that a combination of fluctuations on different timescales can explain changes in seizure network evolution in a regression model in most subjects above chance level.

These results suggest that subject-specific fluctuations in iEEG band power over timescales of minutes to days are associated with how seizures are modulated over time. Future work is needed to link the detected fluctuations to the exact biological time-varying processes. Understanding seizure modulating factors enables development of novel treatment strategies that minimise the seizure spread, duration, or severity and therefore clinical impact of seizures.

1 Introduction

Epilepsy is a common neurological condition characterised by recurrent, unprovoked seizures [1]. It affects approximately 1% of the world’s population and a third of patients experience refractory epilepsy, where seizures are not adequately controlled despite medication.

Importantly, epilepsy is not a static disorder; seizure and pathological brain activities have been shown to fluctuate over hours to years in both intensity and spatial distribution. Specifically, while seizures often share common features in the same patient [2, 3, 4, 5, 6, 7], electrographic seizure dynamics have been shown to change in terms of duration [8], spatial spread [9, 10, 11, 12], spectral properties [13], and wave forms [14] from one seizure to the next. Our recent work [15] has shown that functional network dynamics of epileptic seizures change over time in the same patient. Notably, these changes were consistent with daily (circadian) and/or longer-term fluctuations in most patients [15]. In support of our observations, a recent study quantifying univariate properties of seizure onset and offset also noted that different types of dynamics can be seen across different seizures in the same patient [14]. Similarly, clinical seizure properties are also known to change over time. For example, it is reported that focal seizures, which evolve into bilateral tonic-clonic seizures, preferentially arise from sleep [16]. Subclinical seizures (without clinical symptoms) are also reported to follow circadian patterns [17]. Finally, seizure severity appears to depend on the severity of the preceding seizure in the same patient [18]. Thus, epileptic seizures are not a fully deterministic sequence of abnormal brain activity patterns, but are clearly modulated by processes that shape the neural activity during a seizure and affect seizure severity.

One hypothesis is that this seizure diversity arises from fluctuations in the underlying interictal brain states. It is well-known that spectral properties of the electroencephalogram (EEG) change in each channel from moment to moment [19]. Global and local characteristics of the interictal functional network fluctuate over timescales from hours to days, with circadian rhythm having a particularly strong effect on these dynamics [20, 21, 22]. Interictal fluctuations related to epilepsy have also been reported. For example, high frequency oscillation (HFO) rates vary in location and power within each subject over time [23]. Interictal spikes also change in their location and rate over hours to days [24, 23, 25, 26, 27]. Interestingly, periodicity in interictal spikes over long timescales (days, weeks, and months) has also been found to be associated with seizure occurrence [24, 26, 27]. However, it remains unclear if variability in seizure dynamics are also associated with temporal fluctuations of interictal brain activity on different timescales.

We seek to address this question by exploring what temporal fluctuations of interictal brain activity best explain the diversity in seizure dynamics for each individual subject. Most previous research has focused on analysing spikes, bursts, or HFOs and their association with seizure occurrence. However, an analysis of the factors driving changes in *dynamics* from one seizure to the next is missing. Additionally, we seek to explore the full range of all possible brain activity patterns, which will include epilepsy-related activity patterns (e.g. spikes). Therefore, we analyse temporal fluctuations of continuous iEEG in terms of their spectral properties by detecting subject-specific spatial patterns of band power. We identify which frequency bands and brain areas fluctuate over particular timescales. Finally, we explore whether fluctuations on different timescales are associated with variability in seizure dynamics in each subject.

2 Methods

2.1 Data acquisition

We analysed open source data from people with drug-resistant focal epilepsy (available at <http://ieeg-swez.ethz.ch>). The data consist of a total of 2656 hours of long-term intracranial electroencephalography (iEEG) from 18 subjects. Continuous recordings in each subject cover 24 to 128 channels and vary between 2 to 12 days. More information about the data is given in Supplementary Material. Sampling frequency was either 512 or 1024 Hz depending on the subject. Electrodes (strip, grid, and depth) were implanted intracranially by clinicians. The collection of the data was conducted in the Sleep-Wake-Epilepsy-Center (SWEC) at the University Hospital of Bern, Department of Neurology, as part of their presurgical evaluation programme, independently of this study [28].

iEEG signals were provided in already pre-processed form. Briefly, signals have been median-referenced and band-pass filtered from 0.5-120 Hz using a 4th order Butterworth filter (forward and backward). Seizure onset and termination times were determined by a board-certified epileptologist. Channels with artifacts were also identified and excluded by the same epileptologist. All the steps so far were conducted independently of this study resulting to publicly available data. All patients formally consented to their iEEG data being used for research purposes[28].

2.2 iEEG preprocessing

We performed additional preprocessing steps to extract iEEG band power from the five main frequency bands (Fig. 1a). For each recording channel, the signal was divided into 30 s epochs (Fig. 1b). For each epoch, the band power was computed for the following frequency bands: δ : 1 – 4 Hz, θ : 4 – 8 Hz, α : 8 – 13 Hz, β : 13 – 30 Hz and γ : 30 – 80 Hz. Band power across the five main frequency bands was estimated using Welch’s method for every 30 s epoch, with 1 s sliding window without overlap between consecutive windows. This estimation yielded a time-varying band power, with each time point corresponding to the mean power within a 30 s window. The band power values were aggregated into band-specific matrices with dimensions $\#\text{channels} \times \#\text{epochs}$. Then, these matrices were log transformed and standardised across all epochs and channels within a frequency band. To enable subsequent analysis steps, we also Sigmoid transformed ($S(x) = [1 + \exp(-x)]^{-1}$) the standardised data to ensure positive entries between 0 and 1. For each subject, we then concatenated the matrices from all frequency bands yielding a single $(5 \times \#\text{channels}) \times \#\text{epochs}$ (henceforth defined as $n \times T$; Fig. 1b). We will refer to this matrix as the data matrix X throughout the paper.

2.3 Non-Negative Matrix Factorization for dimensionality reduction

As the data matrix X is high-dimensional with redundant information (e.g. in different channels), we applied a dimensionality reduction step on X using Non-Negative Matrix Factorization (NMF) [29]. NMF provides a low-rank approximation to a non-negative input matrix $X \in \mathbb{R}_+^{n \times T}$ as the product of two non-negative matrices, $W \in \mathbb{R}_+^{n \times k}$ and $H \in \mathbb{R}_+^{k \times T}$, such that $X \approx W \times H \equiv X'$, given an integer k . Specifically, we applied the non-negative singular value decomposition (SVD) with low-rank correction (NNSVD-LRC) [30], which is a method of low-rank approximation using an NMF initialisation approach based on SVD.

In this way, we decomposed each subject’s band power data matrix X into W and H matrices (Fig. 1c-d). Every column of matrix W represents a single NMF component and is a basis vector or feature weight with n elements. Each row of H represents how a single NMF component evolves over time across all T time epochs. We will also refer to a single row of H as the NMF-expression coefficient time series.

To determine the optimal number of representative NMF components, k , we scanned $3 \geq k \geq 15$ in each subject. For each value of k we performed NNSVD-LRC, obtained a W and H and calculated the relative reconstruction errors $\sum_{n,T} |X - X'|/(n \times T)$. We also calculated $c = \max\{\max(|\text{Corr}(W)|), \max(|\text{Corr}(H)|)\}$ for each k , where $\max(|\text{Corr}(W)|)$ represents the maximum absolute correlation among all column pairs of W , and $\max(|\text{Corr}(H)|)$ represents the maximum absolute correlation among all row pairs of H . In other words, we calculated the strongest correlation or anticorrelation between NMF components in terms of their feature weights W and their expression coefficient time series H . In this way, redundant information, particularly in H , was excluded whilst preserving the important spatio-temporal patterns for the next processing steps. We then selected $k = 15$ or the k yielding the smallest correlation between the NMF components that has a relative reconstruction error smaller than 5%, which ever is smaller. Based on this approach, a distinct number of NMF components, k , was selected for each subject.

2.4 Multivariate Empirical Mode Decomposition

After applying NMF with the optimal choice of k , we obtained two matrices for each subject, W and H . To re-iterate, the matrix W consists of the basis vectors, while H is a multivariate time series with dimensions equal to $k \times T$ (= the number of NMF components \times the total number of epochs).

To investigate fluctuations in the band power data on different timescales, we analysed the matrix H using Empirical Mode Decomposition (EMD) [31, 32]. It is well known that EEG signals are non-stationary processes characterised by time-varying features [33, 34]. EMD is a data-adaptive method able to detect non-stationary and non-rhythmic fluctuations on different timescales. EMD decomposes an input signal $Y(t)$, into M finite narrow-band fluctuations, known as intrinsic mode functions (IMFs), based on the local extrema of a time series: $Y(t) = \sum_{i=1}^M \text{IMF}_i(t) + r(t)$, where $r(t)$ is the residue signal [31].

However, local extrema are not directly applicable to multivariate signals [35]. Hence, an extension of the EMD to multi-dimensional space was developed, called the Multivariate Empirical Mode Decomposition (MEMD) [35]. In MEMD, multiple projections of the multivariate signal are generated along different directions in n -dimensional spaces; the multidimensional envelope of the signal is then obtained by interpolating across the different envelopes of these projections [35].

An additional advantage of this method is that it yields the same number of IMFs across the different dimensions of the multivariate signal, and preserves similar frequency fluctuations in the same IMFs across the different dimensions of the signal (mode-alignment) [35].

For the purpose of this analysis, we used MEMD to decompose the NMF-expression coefficient time series, H into a number of multi-dimensional oscillatory modes. Therefore, the matrix H can be represented by the sum of M multi-dimensional IMF signals, where the dimension for each IMF is equal to k (i.e. the number of rows of the matrix H , which corresponds to the number of NMF components). To clarify, we can think of all IMFs in a specific dimension as the decomposition of the corresponding NMF-expression coefficient time series. Thus, $\text{IMF}_{i,j}$ refers to the IMF in the dimension j of the i -th IMF timescale. The j -th NMF-expression coefficient time series $H_j = Y_j(t)$ can be written as $Y_j(t) = \sum_{i=1}^M \text{IMF}_{i,j}(t) + r_j(t)$. This equation applies to every NMF component

$j = 1, \dots, k$.

2.5 Hilbert Spectral Analysis

To obtain a time-frequency representation of the oscillatory modes (IMFs), and hence derive their time-varying characteristics (instantaneous frequency, phase, and amplitude), we applied a Hilbert-transform on each dimension of the IMF (following classical analysis methods for EMD) [31, 32, 36].

For any (real-valued) univariate signal $u(t)$, we can define its Hilbert transform as:

$$H(u)(t) = \frac{1}{\pi} P \int_{-\infty}^{+\infty} \frac{u(\tau)}{t - \tau} d\tau, \quad (1)$$

where P represents the Cauchy principal value for any function $u(t) \in L^P$ class [31].

The analytical signal $v(t)$ obtained from the Hilbert transform can be expressed as:

$$v(t) = u(t) + iH(u)(t) = a(t)e^{i\theta(t)}, \quad (2)$$

where

$$a(t) = \sqrt{u(t)^2 + H(u)(t)^2} \quad (3)$$

and

$$\theta(t) = \tan^{-1} \left(\frac{H(u)(t)}{u(t)} \right) \quad (4)$$

where $a(t)$ and $\theta(t)$ are the instantaneous amplitude and instantaneous phase, respectively.

The instantaneous frequency, $f(t)$, can then be calculated as follows:

$$f(t) = \frac{d\theta(t)}{dt}. \quad (5)$$

The application of EMD along with Hilbert transform leads to the so-called Hilbert-Huang transform. Through the Hilbert spectral analysis, each IMF's instantaneous frequency can be represented as functions of time. The result is a frequency-time distribution of signal amplitude (or energy using the squared values of amplitude, $a^2(t)$), designated as Hilbert amplitude spectrum or Hilbert spectrum (or Hilbert energy spectrum if energy is used instead of amplitude), $H(f, t)$.

For each univariate IMF signal, we can obtain the Hilbert energy spectrum as a function of instantaneous frequency and time mathematically using the following formula:

$$H(f, t) = \begin{cases} a^2(t), & f = f(t) \\ 0, & \text{otherwise.} \end{cases} \quad (6)$$

The Hilbert-Huang marginal spectrum $h(f)$ of the original signal $u(t)$ can then be defined as the total energy distributed across the frequency space within a time period $[0, T]$. Mathematically, this definition can be expressed as shown below:

$$h(f) = \int_0^T H(f, t) dt. \quad (7)$$

By using Equations 6 & 7 we can obtain the Hilbert-Huang marginal spectrum for a univariate IMF signal. However, the application of the multivariate EMD results in multivariate IMF signals. In order to compute the Hilbert-Huang marginal spectrum of each multivariate IMF signal across all dimensions, we simply averaged over the dimensions $H_i(f, t)$ across $i = 1, \dots, k$ dimensions:

$$\bar{H}(f, t) = \frac{\sum_{i=1}^k H_i(f, t)}{k}. \quad (8)$$

The corresponding marginal spectrum $\bar{h}(f)$ was then similarly defined as:

$$\bar{h}(f) = \int_0^T \bar{H}(f, t) dt. \quad (9)$$

For numerical computations, we discretised time t to compute the integrals as sums. Figure 2 shows the marginal Hilbert-Huang spectra for different multivariate IMFs in an example subject.

2.6 Dominant fluctuation frequency in each IMF

For each subject, we determined the dominant fluctuation frequency (measured in cycles/day here) in each IMF, as the one with the highest power based on the marginal Hilbert-Huang spectrum, $\bar{h}(f)$.

2.6.1 Finding a 24h IMF

We will later focus one part of our analysis on IMFs that fluctuate on the time scale of 24 hours (1 cycle/day). To detect those IMFs, we found IMF(s) with a dominant fluctuation frequency of 1 cycle/day. If two IMFs were found (i.e. both displayed the highest power density at 1 cycle/day), then the 24h IMF was determined to be the IMF with the higher power. This case only occurred in 1 subject.

2.7 Relative contribution of iEEG main frequency bands

To understand how much each of the iEEG frequency bands contributed to a certain IMF, we first determined how much each dimension of the IMF contributed to the overall power of the IMF. To this end, we first obtained the mean power E_{ij} in each dimension j of every i -th IMF signal:

$$E_{ij} = \frac{\sum_{t=0}^T a_{ij}(t)^2}{T}, \quad (10)$$

where T is, as before, the number of time epochs, and $a_{ij}(t)$ is the instantaneous amplitude for the j -th dimension of i -th IMF signal at time point t . One of the main properties of MEMD is that multivariate signals are decomposed into multivariate IMF signals of the same dimensions, where all dimensions within an IMF share fluctuations of the same timescale [37]. Hence, focusing on the mean power over time of each dimension within an IMF is a good indication of the power on a particular timescale. The relative contribution of each j -th dimension to the i -th IMF (or relative power) was then defined as:

$$R_{ij} = \frac{E_{ij}}{\sum_{j=1}^k E_{ij}}, \quad (11)$$

with k indicating the number of dimensions.

Using the relative contribution of each dimension as weights, we can then form the weighted sum of all dimensions in terms of contributions of iEEG main frequency bands. The contributions of iEEG main frequency bands is captured in the W matrix across all channels and iEEG main frequency band. By summing channel contributions for each iEEG main frequency band (see

Fig. 3b-c for an example subject), we obtain a matrix of dimensions (# main frequency bands = 5) \times (# dimensions = k). This matrix can now be multiplied with the weight indicating the contribution of each dimension to yield a vector (of length # main frequency bands = 5) indicating the contribution of each main frequency band to particular IMF for each subject.

2.8 Spatial heterogeneity of contributions to each iEEG main frequency band and dimension

To determine if all recording channels contribute homogeneously to a NMF component in a particular frequency band, we used a measure that quantifies sparsity of a distribution: the *Gini index* [38]. Given a vector $\mathbf{x} = (x_1, x_2, \dots, x_N)$ sorted in ascending order such that $x_1 < x_2 < \dots < x_N$, the Gini index can be derived using the following formula:

$$G(\mathbf{x}) = 1 - 2 \sum_{i=1}^N \frac{x_i}{\|\mathbf{x}\|_1} \left(\frac{N-i+\frac{1}{2}}{N} \right). \quad (12)$$

It can range from 0 to 1, with values closer to 0 indicating low sparsity (homogeneity) and values closer to 1 corresponding to higher sparsity (heterogeneity).

We derived the Gini index for each IMF across different channels within each main frequency band. In other word, for each IMF, we first computed the contribution C_i to each i -th IMF as the product of the relative power (eqn. 11) and the weights matrix: $C_i = \sum_j R_{ij} \times W_j$, with i indexing the IMF number, and j indexing its dimension. Specifically, W_j is the j -th column of the W matrix from the NMF decomposition (Fig. 1(c)), whereas R_{ij} is a scalar representing the relative power of the j -th dimension to the i -th IMF (see 2.7). The resulting C_i is a vector of length #frequency bands (= 5) \times #channels, i.e. the same length as W_j . As we are interested in the distribution of each C_i across channels for each frequency band, we applied the Gini index to each frequency band separately in each C_i , yielding one Gini index per frequency band and IMF.

2.9 IMF seizure distance

For each subject, we quantified the difference between pairs of seizures in terms of each IMF. To obtain this difference, we first computed the product $W \times \text{IMF}_i(t)$, where $\text{IMF}_i(t)$ is the multi-dimensional i -th IMF ($k \times T$ matrix). The product yields the matrices X'_{IMF_i} for all $i = 1, \dots, M$ timescales. X'_{IMF_i} reconstructs the i -th IMF in the original space of all channels and frequency bands. For each X'_{IMF_i} , we computed a distance matrix based on the multivariate Euclidean distance of IMF values for each pair of seizures: $D_i(a, b) = \|X'_{\text{IMF}_i}(t_a) - X'_{\text{IMF}_i}(t_b)\|$, where t_a and t_b are the time epochs of the seizure pair's onset. Therefore, we obtained M IMF seizure distance matrices per subject, each representing the pairwise seizure distance for a specific IMF.

Note that any seizure-induced changes in the band power will only be present in a few epochs (as we use 30 s long epochs). Therefore, the seizures are considered to only influence the fastest IMFs (highest-frequency fluctuations), while they should have little effect on the slower IMFs. Supplementary Material additionally shows that our main results were reproduced by using the IMF seizure distances obtained from one epoch before the seizure onset epoch ($t_a - 1$ and $t_b - 1$).

2.10 Seizure dissimilarity

In our previous work, we introduced a quantitative measure of how dissimilar two seizures are within a subject [15]. Briefly, each epileptic seizure in a subject was analysed in terms of its evolution/pathway through the space of functional network dynamics (using exactly the same pipeline as [15]). Each pair of pathways was then compared to each other using dynamic time warping, accounting for different seizures (or parts of seizures) that were very similar in dynamics but not in duration. The average distance between the warped seizures was then taken as the dissimilarity measure. As such, for each subject, we obtained a seizure dissimilarity matrix, which captures the pairwise dissimilarity between seizures of that given subject.

2.11 Association between seizure dissimilarity & IMF seizure distance

In subjects with at least six recorded seizures, we investigated if IMF seizure distances were associated with seizure dissimilarity in each subject. We used a linear regression framework, where the seizure dissimilarity was the response variable and the IMF seizure distances were the explanatory variables. The observations were the dissimilarities and the IMF distances of unique seizure pairs. As each matrix is symmetric, we only used the upper/lower triangular elements to form each variable. We also included the EMD residue signal distances, and temporal distances of seizures (how far apart in time each pair of seizures occurred) as additional explanatory variables. The response, as well as the explanatory variables were standardised individually before fitting the model.

As a variable selection step for our analysis, we used LASSO (Least Absolute Shrinkage and Selection Operator)[39], which is a sparse shrinkage method. Linear regression coefficients were calculated based on least squares, subject to the L_1 penalty. The LASSO also accounted for any collinearity issues between variables. As we were interested in detecting positive relationships between the response variable and the explanatory variables, we used a constrained positive LASSO, that is, coefficients are constrained to be non-negative. Note that only a positive relationship would indicate if seizures are more dissimilar with larger differences in IMF states. The tuning parameter λ for the LASSO model was selected using a 10-fold cross validation method from a range of values $\lambda = 10^{-3}, 10^{-2.95}, \dots, 10^{1.95}, 10^2$ (see Supplementary Material).

After selecting a small number of explanatory variables, an ordinary least squares regression was performed, for each subject, to obtain R^2 and 95% confidence intervals for the coefficients.

2.12 Statistical analysis

In order to assess if the level of explanatory power of the best model selected for each subject has occurred by chance, we performed two separate tests of statistical significance for the adjusted R^2 . Both test yielded the same results and are shown in Supplementary Material

In the first test, we randomly selected seizure onset times by generating a sample from the uniform distribution on the interval $(0, T)$ over 500 iterations. The size of the sample was equal to the number of annotated seizures for each iteration. Then, for every sample of seizure onset times, we obtained new IMF seizure distance matrices and we performed the LASSO and linear regression, as described in the previous section, leaving the response variable unchanged. Finally, we calculated the adjusted R^2 for each iteration. Across all iterations, the adjusted R^2 values were used to estimate the distribution of the test statistic used in the permutation test. P-values were then calculated as the percentage of adjusted R^2 values that were larger in the permutation

distribution. Statistical significance was determined based on a significance level of 5%.

In the second test, we permuted the order of the seizures without permuting the seizure timing over 500 iterations. We then performed the LASSO and subsequent steps like in the first test.

2.13 Data and code availability

The long-term iEEG recordings for all patients are available at <http://ieeg-swez.ethz.ch/> under the section “Long-term Dataset and Algorithms” [28].

Initial signal processing was performed using Matlab version 2019a and Matlab’s built-in functions. NMF and MEMD were implemented using the following publicly available functions:

- **Non-negative matrix factorisation** was conducted using the NNSVD-LRC function from <https://sites.google.com/site/nicolasmillis/code> [30].
- **Multivariate empirical mode decomposition** was applied using code from <http://www.commsp.ee.ic.ac.uk/~mandic/research/emd.htm> [35].

For the remainder of the analysis and the construction of all figures we used Python version 3.5. Either standard functions obtained from published libraries supported by Python were used or custom code written in Python. The main functions used in the analysis are listed below:

- **Hilbert transform:** `scipy.signal.hilbert`
- **LASSO:** `sklearn.linear_model.Lasso`
- **k-fold cross-validation:** `sklearn.model_selection.kFold`

For fitting **linear regression** models, we used the `lm` function from `stats` package implemented in RStudio version 1.1.463 using R version 3.6.3.

Our analysis code and data (post processing) can be found on <https://github.com/cnnp-lab/> (will be added).

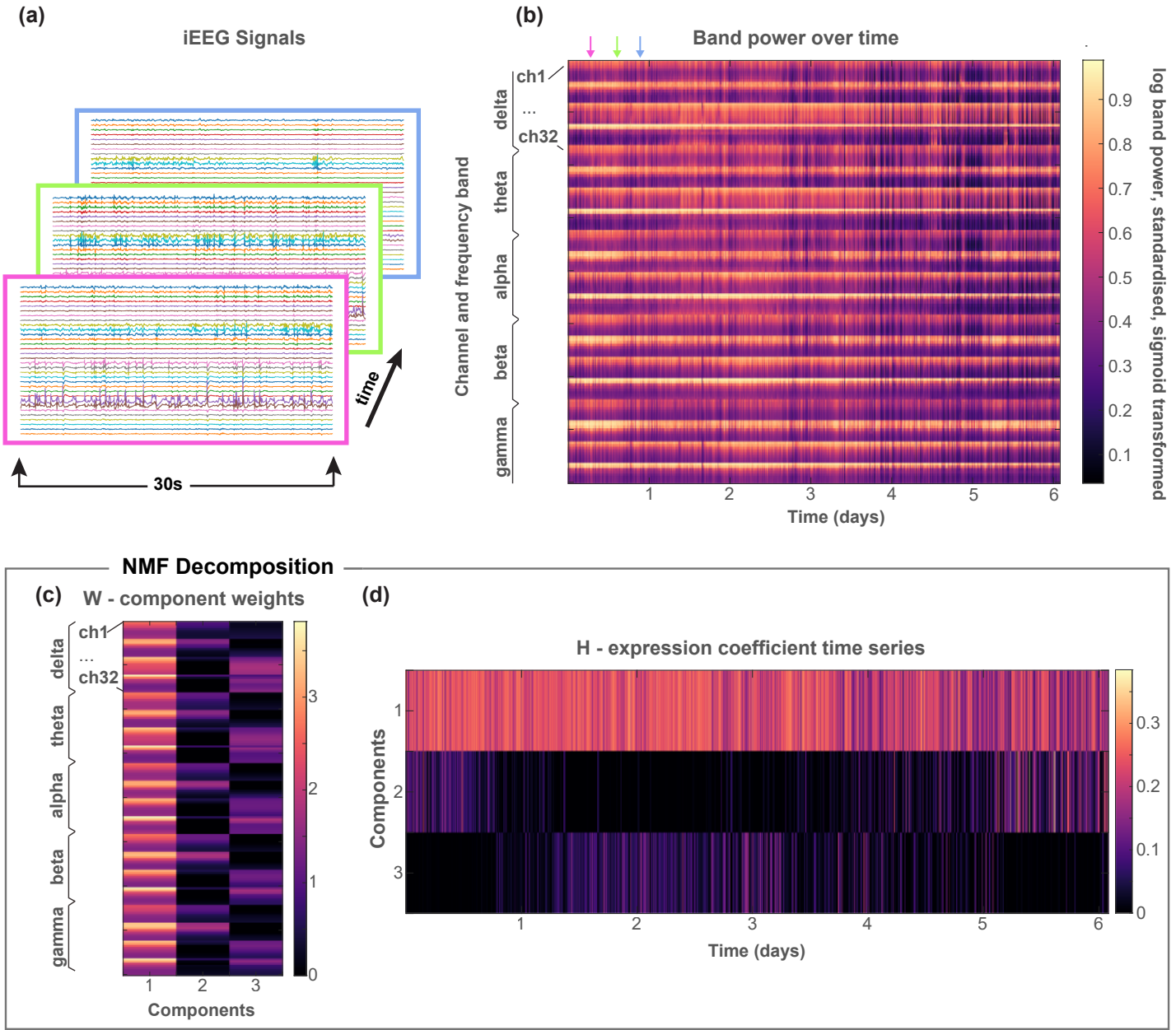


Figure 1: Workflow of data pre-processing; calculation of band power and NMF implementation. (a) 30 s segments were extracted along the recording from the multi-channel iEEG. (b) The standardised, log and sigmoid transformed band power. (c)&(d) NMF of the band power matrix results in the decomposition $W \times H$. (c) The matrix W contains the basis vectors, each of which had $5 \times \#channels$ weights that represents a pattern of frequency across all channels and frequency bands. (d) The coefficients matrix H captures the contribution of each frequency pattern (basis vector) to each time window.

3 Results

We analysed the band power of multi-channel iEEG signals in five main frequency bands in terms of their underlying temporal fluctuations on various timescales for 18 subjects with focal epilepsy. We investigated if fluctuations on particular timescales were driven by particular iEEG frequency bands or spatially localised activity. We then explored if these temporal fluctuations are associated with how seizures change within subjects.

3.1 iEEG band power patterns fluctuate on different timescales

After extracting band power in the frequency bands ($\delta, \theta, \alpha, \beta, \gamma$) in 30 s sliding windows (no overlap) for each iEEG channel (Fig. 1a,b), we performed dimensionality reduction using a non-negative matrix factorisation (NMF) approach. NMF effectively groups channels and frequency bands to form components that can be added together to approximately reconstruct the data. Weights for each component are shown in matrix W , Fig. 1c. The expression coefficients of these components at each time point is then given by the H matrix, which essentially yields a time series for each component (Fig. 1d). The set of coefficient time series in H show the fluctuations of particular patterns of band power and channels over time.

For each subject, we then used Multivariate Empirical Mode Decomposition (MEMD) to determine the different timescales of fluctuations for each NMF coefficient time series. Figure 2a shows the MEMD results for a single NMF component in example subject ID06, yielding 15 Intrinsic Mode Functions (IMFs) and a residue signal in this case. Faster IMFs (e.g., IMF1, 2 and 3) are often thought to contain noise, but might also reflect genuine fluctuations in the initial signal (Supplementary Material). However, for simplicity, we will retain all IMFs for the subsequent main results, and refer the reader to Supplementary Material for a more detailed supplementary analysis.

Using the instantaneous frequency and amplitude through the Hilbert transform, we obtained a representation of the marginal spectral densities of each IMF in each dimension. Figure 2b shows the marginal spectral densities averaged across all dimensions for each IMF (blue lines) for example subject ID06. Some distinct peaks are seen especially in the slower IMFs, e.g. IMF13 (at ≈ 1 cycle/day), IMF14 (at ≈ 0.3 cycle/day), IMF9 (≈ 8 cycles/day), IMF8 (≈ 15 cycles/day), etc. Note that both EMD and MEMD as methods essentially acts as a dyadic filter bank [40, 41, 42], thus the dyadic pattern seen in the faster IMFs is not surprising.

All subjects had band power fluctuations with a 24h cycle (Fig. 2c), while fluctuations on other timescales were more subject-specific in cycle length. For 10 out of 18 subjects (ID01, ID02, ID07, ID08, ID09, ID11, ID12, ID13, ID17 and ID18) the 24h cycle had the highest density (Fig. 2d). For six subjects (ID03, ID04, ID05, ID14, ID15 and ID16) the 24h cycle was slightly lower in density, as the highest density was seen in slower or faster IMFs. For two subjects (ID06 and ID10) the 24h cycle did not feature in the top three highest densities, but a peak at 24h can still be observed in ID06 (Fig. 2c).

3.2 All iEEG frequency bands contribute to the 24h IMF

Following the observation of a 24h cycle in all subjects, we want to assess the contribution of each iEEG frequency band to this 24h fluctuation. We first determined the 24h IMF, which is IMF 13 in example subject ID06 (Fig. 3a). We then calculated the relative power in each dimension of the IMF, each of which corresponds to an NMF component. For example, in subject ID06, the

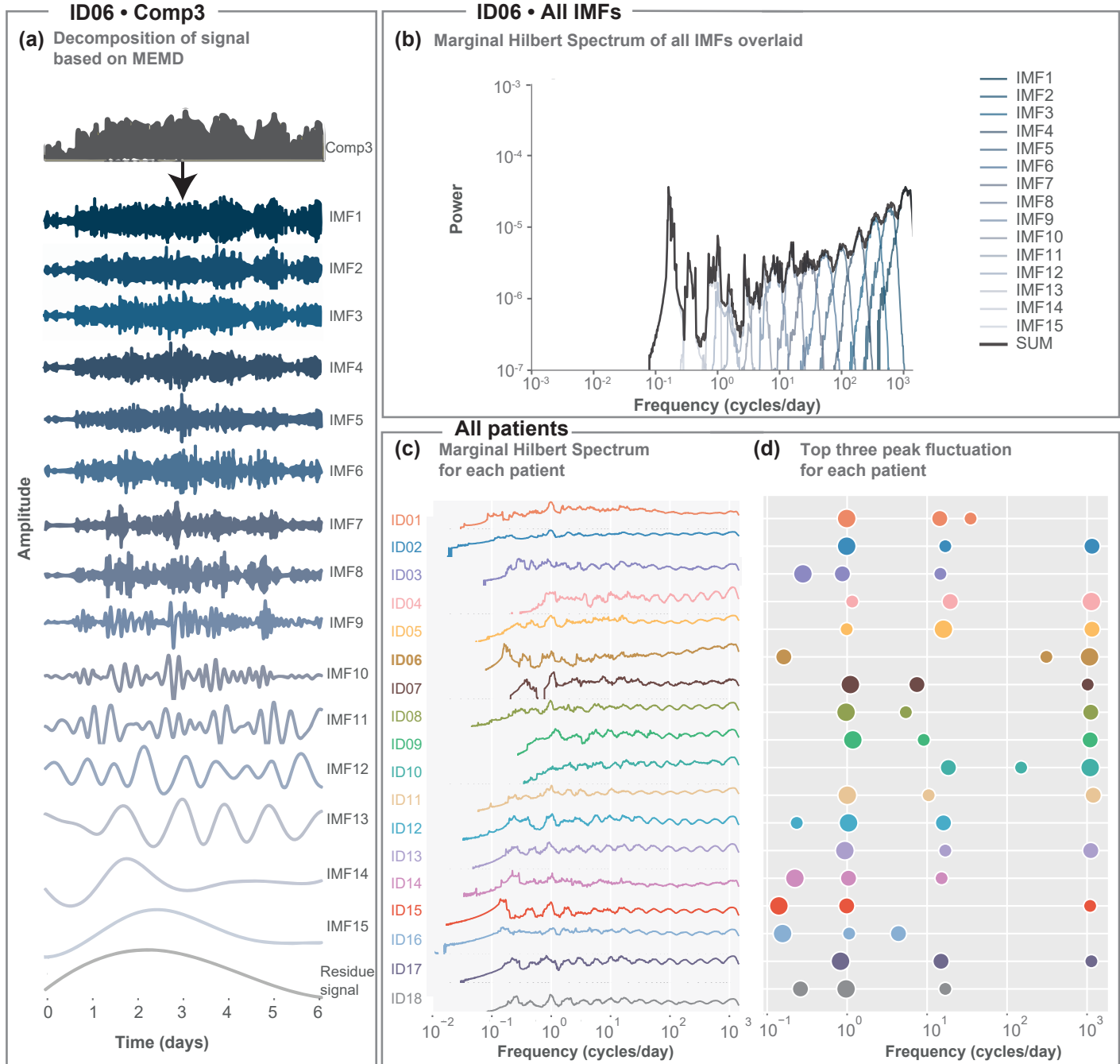


Figure 2: MEMD detects fluctuations on different timescales for each subject. (a) MEMD yields 16 IMFs in example subject ID06. Only one dimension of the IMF (corresponding to the first NMF component) is shown for simplicity. IMFs are presented in ascending order (fastest to slowest, top to bottom). The last trace is the residue signal (b) Marginal Hilbert spectrum of instantaneous frequencies for all IMFs (aggregated across all dimensions) in example subject ID06. The black line represents the Marginal Hilbert frequency spectrum across all IMFs. (c) Marginal Hilbert frequency spectrum across all IMFs for each subject. (d) Bubble plot of peak fluctuations for the three highest power densities according to the Marginal Hilbert frequency spectrum across all IMFs for each subject. The size of the bubbles indicates the first, second and third peak in descending order.

majority of its power (54%) is concentrated in dimension 1 (Fig. 3a). We also noted that the 24h fluctuation does not follow the same phase in all dimensions of the IMF, potentially indicating the presence of multiple processes fluctuating on a 24h timescale. Since we are interested in the overall contribution of each frequency band to the 24h cycle, we decided to assess the contribution of different frequency bands over all dimensions next.

From the dimensionality reduction step, we already know the weights across all iEEG frequency bands and channels (matrix W , see Fig. 3b). For each NMF component, we computed the weight of each frequency band by summing the weights of that frequency band across all channels (Fig. 3c). Finally, a sum weighted by the relative power in the IMF over all dimensions was obtained representing the relative contribution of each frequency band to the IMF. For most subjects, δ band power contribution was slightly higher compared to the other frequency bands for the 24h cycle IMF. However, other frequency bands also contributed to the 24h cycle IMF in most subjects (Fig. 3d).

3.3 Groups of channels contribute to IMFs slower than 24h

Within each frequency band we also investigated the contribution of each channel to an IMF. Specifically, we investigated if the contributions were similar or heterogeneous across all channels. We used the Gini index as a measure of spatial heterogeneity, where 0 (1) indicates a completely homogeneous (heterogeneous) channel contribution for each IMF. Figure 4 shows the distribution of Gini indices of all IMFs in the δ band across all subjects, where IMFs are grouped by the IMF dominant frequency of fluctuation. Results for other iEEG main frequency bands are similar and shown in Supplementary Material. Overall, the Gini indices are low for all IMFs, indicating that IMFs are not driven by a small group of channels. However, there is a clear tendency for slower IMFs (below 1 cycle per day) to display a higher Gini index, indicating that slower fluctuations may be driven by a group of channels.

3.4 Band power IMF fluctuations are associated with seizure dissimilarity in most subjects

As the final part of our analysis, we investigated if these fluctuations on different timescales detected in the IMFs are associated with our recent observation of changes in seizure properties over time in individual subjects [15]. Particularly, we previously showed that seizure network dynamics change over time in every subject, and that these changes could be explained by hypothetical circadian or longer timescale modulators. Here, we explored if the subject-specific fluctuations detected by the IMFs are associated with changes in seizure dynamics.

For each IMF in each subject, we first determined their corresponding seizure IMF Euclidean distance matrix (Fig.5a,b). For example, in subject ID06's IMF 6, we calculated the Euclidean distance of every time point to the time point of the first seizure (Fig.5a) across all dimensions. By reading out all the Euclidean distances to all the other seizure time points, we obtained the first row of the seizure IMF Euclidean distance matrix (Fig.5b). The same process was repeated for all other seizures in this subject. This distance matrix has dimensions of number of seizures by number of seizures and represents how different the IMF state is for each seizure pair.

By using the same techniques as in [15], we obtained a seizure dissimilarity matrix, which expresses how dissimilar each pair of seizure pathways are through the space of network dynamics (Fig.5c,d). The seizure dissimilarity matrix represents how each pair of seizures differ within a

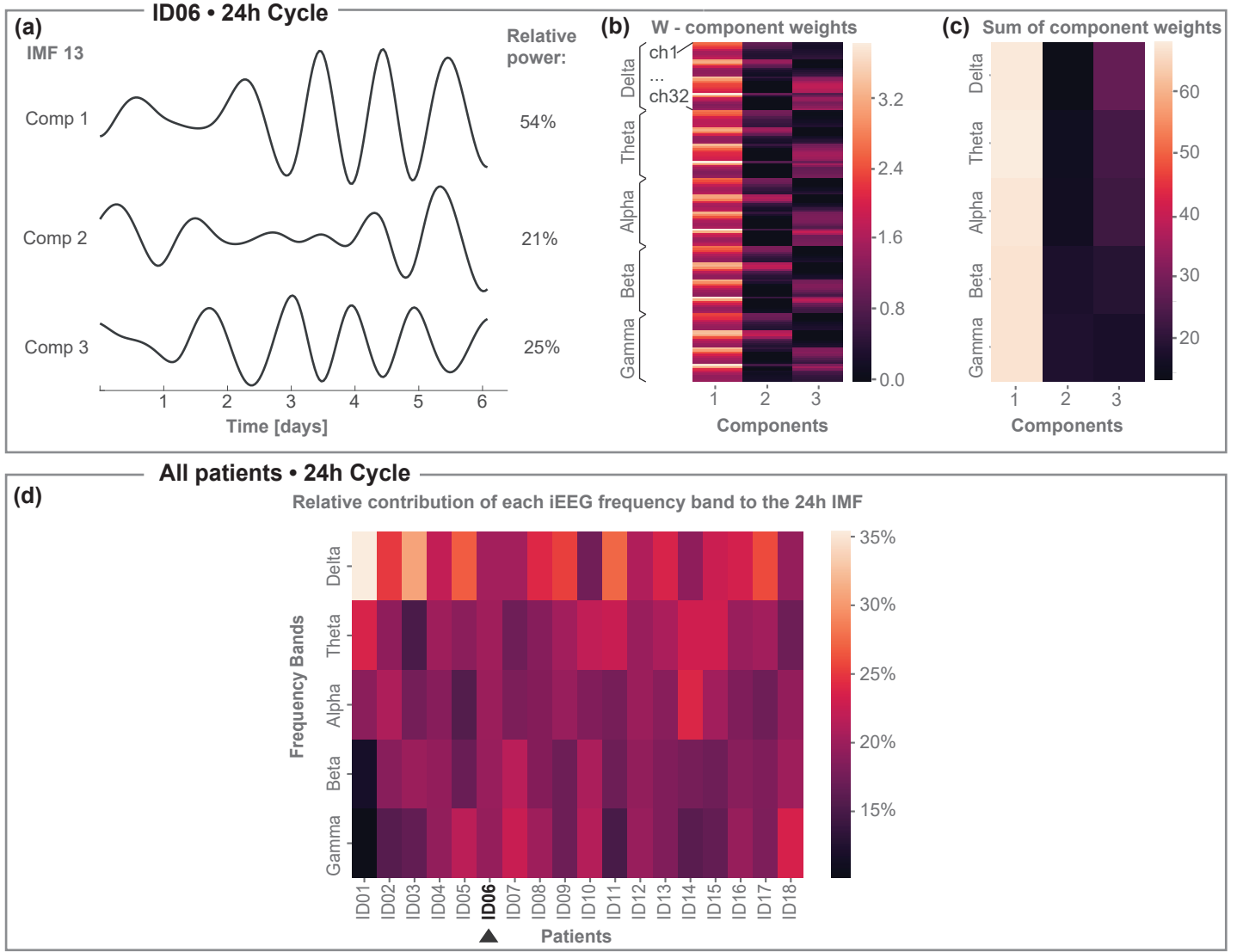


Figure 3: Contribution of iEEG main frequency bands to the 24h IMF. (a) IMF 13 in example subject ID06 shows fluctuations on the scale of 24h across all three dimensions (each of which corresponds to an NMF component). Dimension 1 shows the highest relative power in this IMF. (b) W component weight matrix (same as Fig. 1c). (c) The sum of the component weights across all channels within each frequency band. (d) Contribution of each iEEG frequency band to the 24h IMF across all subjects obtained by forming the sum over the matrix in (c) weighted by the relative power in (a). To be able to compare subjects to each other, each column here has been normalised to form a percentage contribution.

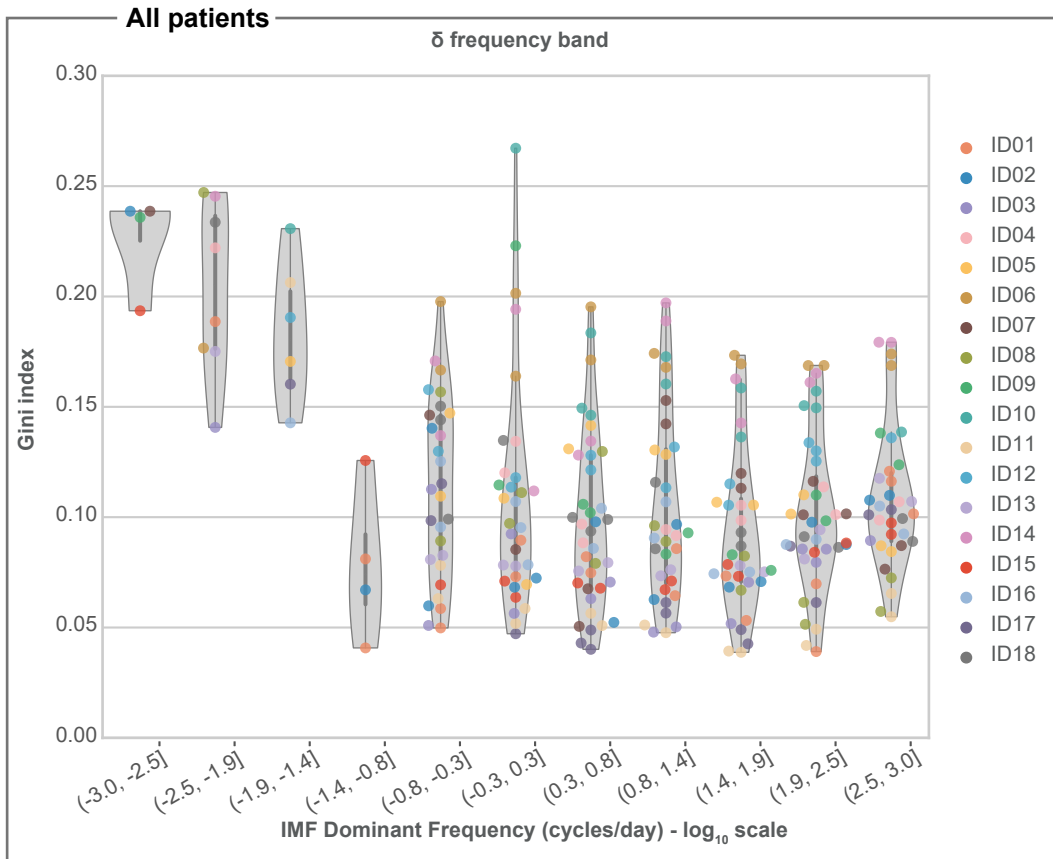


Figure 4: Gini index of IMFs for the δ frequency band across all subjects. Across all subjects, we grouped IMFs based on their dominant IMF frequency and show the distribution of the corresponding Gini indices as a violin plot with enclosed box plot. The thick grey bar represents the inter-quartile range.

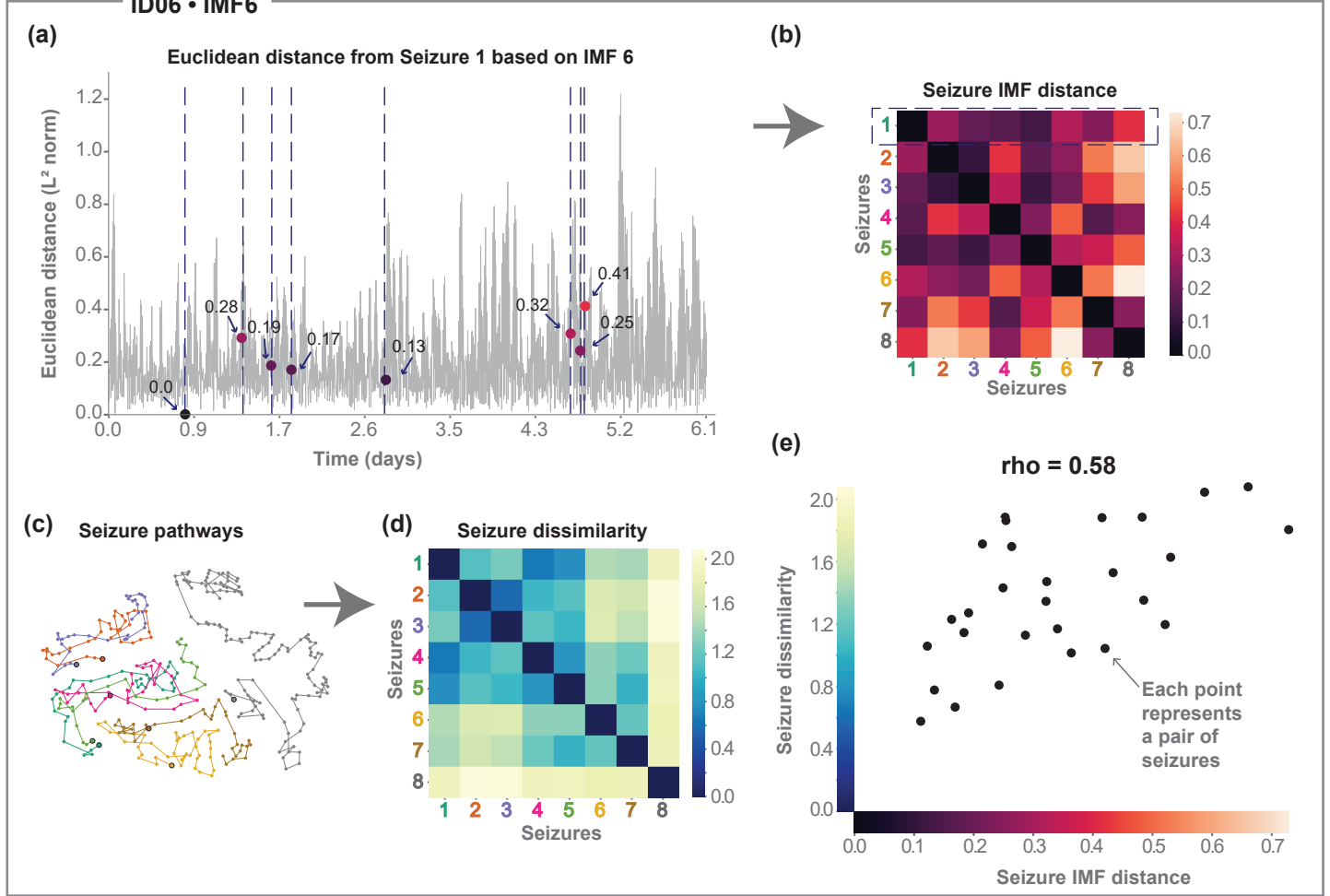


Figure 5: Relating seizure dissimilarity and IMF seizure distance. Throughout the figure we use example subject ID06 and IMF 6. (a) Euclidean distance of all time points to the first seizure in terms of IMF 6. Blue dashed vertical lines indicate seizure timing. Dots mark the value of the IMF distance to the first seizure and colours of dots correspond to the colour scale in (b). (b) Seizure IMF distance matrix for IMF 6. The first row is a representation of the data in (a). (c) Seizure pathways derived from seizure EEG (see Supplementary Material). Similar seizures tend to be placed closer together in this projection. Seizures are displayed with distinct colours to distinguish seizure events. The starting points of seizures are marked with a black outline circle. (d) Seizure dissimilarity matrix, capturing the differences in seizure pathways over time between each pair of seizures. (e) Scatter plot of seizure dissimilarity and the seizure IMF distance (Spearman's correlation, $\rho = 0.58$).

subject. By relating the set of seizure dissimilarities to the corresponding set of IMF Euclidean distance, we then investigated if there is an association between the two Fig.5(e).

To generalise this approach to all IMFs in a subject, we fitted a multiple linear regression model, where the sets of seizure IMF distances (derived from different IMFs) are explanatory variables, and the seizure dissimilarity is the response variable (Fig.6a). We also included the EMD residue signal and temporal distance between seizures (i.e. how far apart in time each seizure pair occurred) as explanatory variables to model fluctuations of longer timescales than the recording time. The observations are pairs of seizures. We fitted a model for each subject

with at least six seizures. After LASSO variable selection and linear regression, the estimated regression coefficients for example subject ID06 are shown in Fig.6(c). The strongest explanatory effect (as measured by the standardised regression coefficients, also known as beta-weights) was seen in the EMD residue signal followed by some faster IMFs (IMF3, 4, 5 and 6). For this particular subject, according to the model, 67.42% of the variability of seizure dissimilarity was explained by explanatory variables (i.e. adjusted $R^2 = 0.6742$).

Out of our cohort of eight subjects, six had an adjusted R^2 around or above 0.6 (Fig.6d). Supplementary Material additionally shows that the adjusted R^2 values would have not occurred by chance, except for ID10. For 6 out of 8 subjects, IMFs around 24h were also part of the explanatory variables (Fig.6d). Faster than 24h IMFs also tended to remain as explanatory variables in the models for all subjects. Temporal distance between seizures remained as an explanatory variable in three subjects, and the residue signal also remained as an explanatory variable in three additional subjects. Overall, a subject-specific combination of different fluctuations were sufficient to provide a good explanation of seizure variability in most subjects.

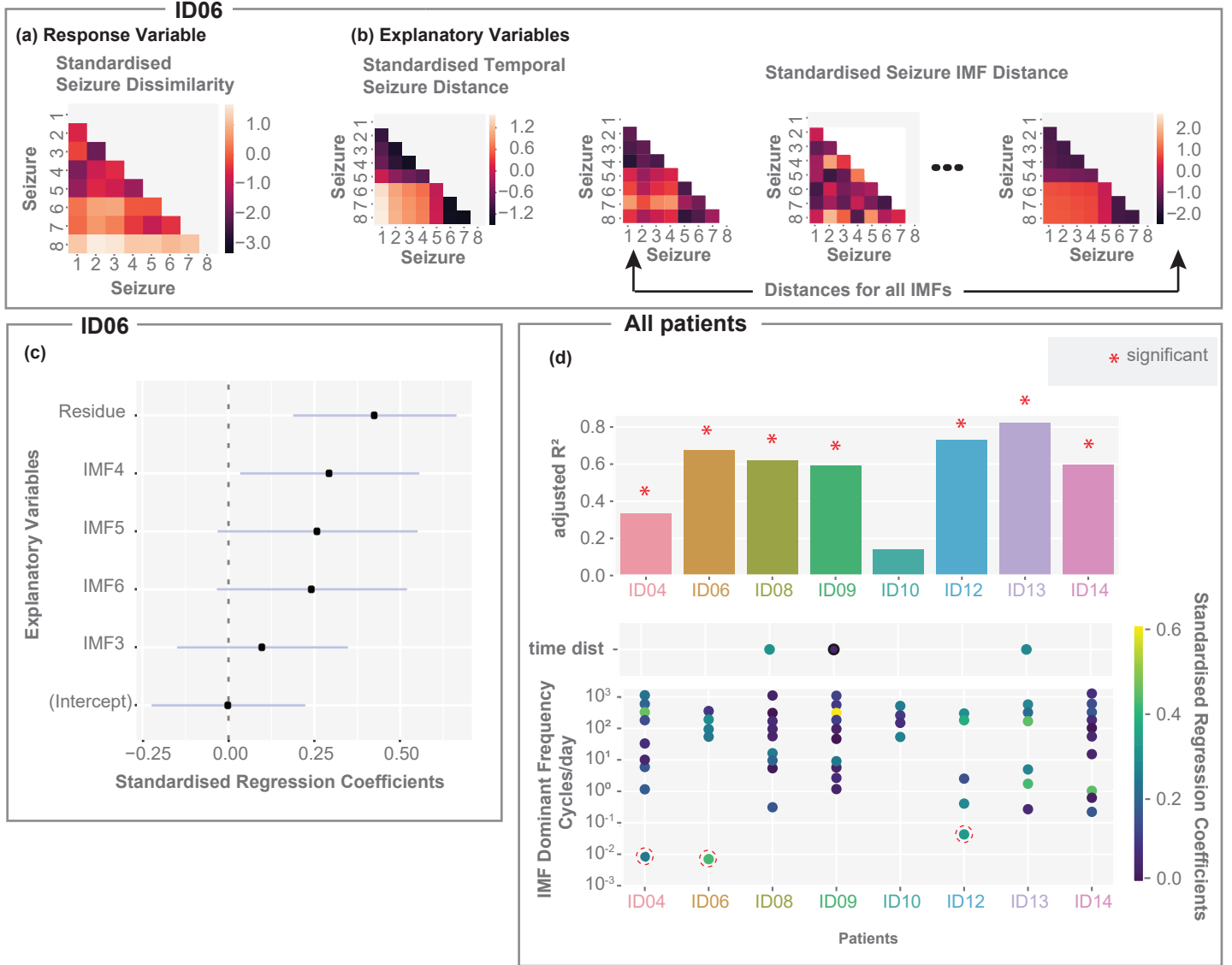


Figure 6: A combination of IMF seizure distances on different timescales can explain seizure dissimilarity in most subjects in a multiple regression model. (a) Standardised seizure dissimilarity matrix (response variable). Only the lower triangle of the symmetric matrix is shown, where each entry serves as an observation. (b) Explanatory variables: The matrix on the left shows the standardised temporal seizure distance. Each entry corresponds to the absolute time difference between seizures. The remaining matrices are standardised seizure IMF distance matrices. (c) Coefficient estimates (black dots), based on ordinary least squares regression for ID06, with lines indicating 95% confidence intervals. Only five explanatory variables were left after performing variable selection based on constrained LASSO. (d) Summary across subjects based on Ordinary Least Squares (OLS) models with explanatory variables obtained by the constrained LASSO. Top: Bar chart of the adjusted R^2 . Red stars indicate p -values ≤ 0.05 . Bottom: Dot plot indicating the OLS coefficient estimates for the time distance (when this variable remained in the model) together with OLS coefficient estimates at the corresponding value of IMF dominant frequency for each subject. In case the model included the residue, its coefficient estimate was circled with a dashed red line; the dominant frequency of the residue cannot be accurately determined, but only indicated.

4 Discussion

We demonstrated that long-term iEEG signal band power fluctuates over a range of timescales (from minutes to days), and a subject-specific combination of such fluctuations provide a good explanation (adjusted $R^2 \geq 0.6$) for how seizure dynamics change over time in most subjects.

Fluctuations on various timescales of the continuous EEG have been reported in several studies using iEEG recordings. The prevalence of a strong circadian rhythm in EEG patterns has long been shown [43, 44, 45, 46, 47]. Weaker ultradian (more than 1 cycle per day) rhythms have also been reported in long-term EEG band power during daytime wakefulness in healthy subjects [48, 49]. For example, ultradian modulations are reported to occur with a cycle of two and four hours in the 9-11 Hz and 11-13 Hz frequency bands, respectively [48]. Using a functional connectivity measure of EEG, [22] also reported ultradian fluctuations in addition to a strong circadian rhythm. Recently, subject-specific multidien (multi-day, i.e. less than 1 cycle per day) rhythms have been detected in the rate of interictal epileptiform activity in epilepsy subjects [26, 24]. Similarly, daily and longer cycles were shown in the variance and autocorrelation of EEG signals [50]. In agreement, we observed the 24h cycle in all subjects, and additional fluctuations on ultradian and multidien timescales that were subject-specific.

We additionally made two observations about these fluctuations on different timescales. First, we saw that different frequency bands appear to contribute to a similar degree to the circadian fluctuation of iEEG band power, although subtle subject-specific patterns of contribution were also noted. However, our analysis was performed across all dimensions of our data. The different dimensions of the IMF can display phase and amplitude differences (see e.g. Fig. 3a), indicating that different circadian fluctuations (with different phases) exist in each subject, as has been reported before [46]. Future work may wish to investigate the frequency contributions to different dimensions of IMFs and also relate those IMFs to other physiological variables such as body temperature or plasma melatonin [46].

The second observation we made was that slower (multidien) fluctuations tended to arise from groups of channels, whereas faster (circadian and ultradian) fluctuations tended to arise as a more equal contribution from all channels. Again, similar to our first observation, we also performed our analysis over all dimensions of the IMFs. Individual dimensions of IMFs may have more spatially heterogeneous contributors. A limitation in our analysis is that iEEG often only provides limited spatial coverage, and the electrode layout is patient-specific. However, information on the location of the electrodes was not available as part of the SWEC-ETHZ iEEG dataset. To fully uncover the spatial and frequency band contributions to each dimension of each IMF, we suggest that future work should consider the spatial location of the iEEG and perform an iterative combination of dimensionality reduction and empirical mode decomposition to find components and their contributions for each IMF. From a clinical perspective, information on the spatial coverage and location of the electrodes would further allow us to investigate the overlap of the location of these temporal fluctuations with the epileptogenic zone in focal epilepsies.

Our main goal was to investigate if there is an association between seizure dissimilarity and fluctuations in long-term iEEG band power. Seizure dissimilarity is a measure that was proposed to assess how different any pair of seizures are in a given subject in terms of their seizure evolution. Previous work has also shown that seizure dissimilarity was well-explained by processes incorporating Gaussian noise, circadian and/or slower timescales of changes in most subjects [15]. In agreement, we found that circadian or multidien fluctuations contributed strongly in most subjects in explaining seizure dissimilarity. Interestingly, we also found many faster (ultradian) fluctuations as explanatory variables in most subjects. These fluctuations could be contributing

explanatory power through what previously was modelled as noise [15]. With larger datasets using more seizures recorded over a longer period, future work should investigate ultradian contributions carefully and assess if noise would perform as well as the cumulative ultradian contributions.

It is worth noting that while fluctuations in long-term iEEG band power can explain seizure dissimilarity fairly well, this association should not be interpreted as causal evidence. The observed band power fluctuations can be understood as signatures of multiple biological processes, which could directly dictate seizure dynamics or be co-modulated by the same upstream processes as the seizure dynamics. Our data cannot distinguish these two cases. Alternative fluctuations (not captured by iEEG band power) may additionally explain seizure dissimilarity, and a more detailed analysis of the exact fluctuations and the differences in specific seizure features may be more informative. We also wish to point out that the band power fluctuations did not account for all the seizure variability in most subjects. The highest adjusted R^2 was around 0.8 and the unexplained variability based on the models suggests that there are additional factors that impact seizure dynamics. Nevertheless, to make our findings clinically useful, e.g. as a predictive model of upcoming seizure dynamics or seizure severity, neither causality, nor completeness of the predictors is required. In other words, our results indicate that a predictive model of seizure dynamics is possible with interictal features such as iEEG band power, and should achieve good predictive performance in the majority of subjects.

To improve predictive performance, other factors could be considered in future, e.g. the anti-epileptic drug (AED) level at any given time, stochastic elements of seizure evolution (e.g. seizure termination) [51], or additional interictal features that we don't consider in our analysis (e.g. interictal network dynamics). Specifically, it is well-known that AED changes and withdrawal can change the severity and dynamics of seizures. For example, bilateral tonic-clonic seizures are more prevalent when AED levels are reduced [12]. We were unable to include this information in the current study, but future studies may wish to investigate how AED levels impact iEEG band power [52], in combination with their potential explanatory power for seizure dissimilarity.

In the context of epilepsy treatments, it is worth stating that any discovered three-way association between interictal brain activity, seizure dynamics, and treatments (such as AEDs, or epilepsy surgery) has the potential to introduce entirely new treatment strategies. If, for example, particular interictal EEG signatures predict more severe seizures, and these signatures are also influenced by AED dose, then one can hypothesise that adapting AED dose according to these interictal signatures might decrease seizure severity. If the hypothesis can be verified, then on-demand drug-delivery systems programmed to respond to (patient-specific) interictal signatures could become the next generation of epilepsy treatments.

In a more general context, our work is another contribution to the wider literature of explaining ictal features from interictal EEG features or hypothesised circadian/multidien rhythms. Most notably, the ictal feature of interest is often the seizure timing (when a seizure occurs). For example, studies have established that there is often a subject-specific relationship between fluctuations of interictal EEG features and the timing of ictal events [26, 24, 22]. A number of studies also demonstrated that seizure occurrence is underpinned by circadian/multidien rhythms [26, 24, 53, 54, 44]. Interestingly, we found no evidence of an association between band power fluctuations of the interictal EEG and seizure occurrence (data not shown). Seizures were not more likely to occur during particular phases of particular IMFs in most subjects in our data set. This is in agreement with a previous study [22] that reported functional network fluctuations, rather than band power fluctuations, to be more predictive of seizure timing. Future work should investigate temporal fluctuations in a range of EEG features, such as band power [47], functional connectivity [22], high frequency oscillations [23], variance, and autocorrelation [50]. Apart from seizure timing, our work

has shown that band power fluctuations on different timescales of the interictal EEG also explain seizure network evolutions. Future work should explore this avenue further to illuminate the exact processes and timescales that modulate or dictate the various aspects of a seizure.

A variety of internal and external factors are known to fluctuate on different timescales and modulate epileptic processes. External factors may be environmental processes such as lower atmospheric pressure, high air humidity and temperature [55] or processes related to nutrition, such as caffeine [56]. Potential internal factors, which can also be influenced by external factors, include emotional/physical stress [57], low quality of sleep [58], and fatigue [59]. Other internal factors include hormonal rhythms (e.g. menstrual cycles) [60, 61] and circadian rhythms [62]. Seizure frequency, seizure dynamics, interictal epileptic phenomena (e.g. spikes, bursts, HFOs) and general interictal EEG patterns all might be affected by these time-varying factors [63, 64, 65]. However, additional studies are needed to unravel the exact, and possibly patient-specific relationship between modulators and epileptic processes.

In conclusion, seizure occurrence may not be the only aspect of a seizure that is correlated with fluctuating interictal EEG features. Our work has shown that the seizure dynamics are associated with such interictal fluctuations on multidien, circadian, and ultradian timescales. As such, EEG fluctuations on different timescales may be able to predict seizure dynamics in future. Prediction of various seizure features, including seizure evolution and seizure severity, would be highly desirable to improve quality of life for patients. Furthermore, if a causal link can be demonstrated between the interictal fluctuations and seizure features, manipulating interictal dynamics could become a novel approach for reducing seizure severity.

References

- [1] C. E. Stafstrom and L. Carmant, “Seizures and Epilepsy: An Overview for Neuroscientists,” *Cold Spring Harbor perspectives in medicine*, vol. 5, p. a022426, June 2015.
- [2] M. A. Kramer, U. T. Eden, E. D. Kolaczyk, R. Zepeda, E. N. Eskandar, and S. S. Cash, “Coalescence and Fragmentation of Cortical Networks during Focal Seizures,” *Journal of Neuroscience*, vol. 30, pp. 10076–10085, July 2010.
- [3] K. Schindler, H. Gast, L. Stieglitz, A. Stibal, M. Hauf, R. Wiest, L. Mariani, and C. Rummel, “Forbidden ordinal patterns of periictal intracranial EEG indicate deterministic dynamics in human epileptic seizures,” *Epilepsia*, vol. 52, no. 10, pp. 1771–1780, 2011.
- [4] C. A. Schevon, S. A. Weiss, G. McKhann, R. R. Goodman, R. Yuste, R. G. Emerson, and A. J. Trevelyan, “Evidence of an inhibitory restraint of seizure activity in humans,” *Nature Communications*, vol. 3, p. 1060, Sept. 2012.
- [5] S. P. Burns, S. Santaniello, R. B. Yaffe, C. C. Jouny, N. E. Crone, G. K. Bergey, W. S. Anderson, and S. V. Sarma, “Network dynamics of the brain and influence of the epileptic seizure onset zone,” *Proceedings of the National Academy of Sciences*, vol. 111, pp. E5321–E5330, Dec. 2014.
- [6] F. B. Wagner, E. N. Eskandar, G. R. Cosgrove, J. R. Madsen, A. S. Blum, N. S. Potter, L. R. Hochberg, S. S. Cash, and W. Truccolo, “Microscale spatiotemporal dynamics during neocortical propagation of human focal seizures,” *NeuroImage*, vol. 122, pp. 114–130, Nov. 2015.

- [7] W. Truccolo, J. A. Donoghue, L. R. Hochberg, E. N. Eskandar, J. R. Madsen, W. S. Anderson, E. N. Brown, E. Halgren, and S. S. Cash, “Single-neuron dynamics in human focal epilepsy,” *Nature Neuroscience*, vol. 14, pp. 635–641, May 2011.
- [8] M. J. Cook, P. J. Karoly, D. R. Freestone, D. Himes, K. Leyde, S. Berkovic, T. O’Brien, D. B. Grayden, and R. Boston, “Human focal seizures are characterized by populations of fixed duration and interval,” *Epilepsia*, vol. 57, no. 3, pp. 359–368, 2016.
- [9] M. G. Marciani and J. Gotman, “Effects of Drug Withdrawal on Location of Seizure Onset,” *Epilepsia*, vol. 27, no. 4, pp. 423–431, 1986.
- [10] P. A. Karthick, H. Tanaka, H. M. Khoo, and J. Gotman, “Prediction of secondary generalization from a focal onset seizure in intracerebral EEG,” *Clinical Neurophysiology*, vol. 129, pp. 1030–1040, May 2018.
- [11] J. S. Naftulin, O. J. Ahmed, G. Piantoni, J.-B. Eichenlaub, L.-E. Martinet, M. A. Kramer, and S. S. Cash, “Ictal and Preictal Power Changes Outside of the Seizure Focus Correlate with Seizure Generalization,” *Epilepsia*, vol. 59, p. 1398, July 2018.
- [12] M. C. Pensel, M. Schnuerch, C. E. Elger, and R. Surges, “Predictors of focal to bilateral tonic-clonic seizures during long-term video-EEG monitoring,” *Epilepsia*, vol. 61, no. 3, pp. 489–497, 2020.
- [13] G. Alarcon, C. D. Binnie, R. D. C. Elwes, and C. E. Polkey, “Power spectrum and intracranial EEG patterns at seizure onset in partial epilepsy,” *Electroencephalography and Clinical Neurophysiology*, vol. 94, pp. 326–337, May 1995.
- [14] M. L. Saggio, D. Crisp, J. M. Scott, P. Karoly, L. Kuhlmann, M. Nakatani, T. Murai, M. Düm-pelmann, A. Schulze-Bonhage, A. Ikeda, M. Cook, S. V. Gliske, J. Lin, C. Bernard, V. Jirsa, and W. C. Stacey, “A taxonomy of seizure dynamotypes,” *eLife*, vol. 9, July 2020.
- [15] G. M. Schroeder, B. Diehl, F. A. Chowdhury, J. S. Duncan, J. d. Tisi, A. J. Trevelyan, R. Forsyth, A. Jackson, P. N. Taylor, and Y. Wang, “Seizure pathways change on circadian and slower timescales in individual patients with focal epilepsy,” *Proceedings of the National Academy of Sciences*, May 2020.
- [16] B. C. Jobst, P. D. Williamson, T. B. Neuschwander, T. M. Darcey, V. M. Thadani, and D. W. Roberts, “Secondarily Generalized Seizures in Mesial Temporal Epilepsy: Clinical Characteristics, Lateralizing Signs, and Association With Sleep–Wake Cycle,” *Epilepsia*, vol. 42, no. 10, pp. 1279–1287, 2001.
- [17] B. Jin, S. Wang, L. Yang, C. Shen, Y. Ding, Y. Guo, Z. Wang, J. Zhu, S. Wang, and M. Ding, “Prevalence and predictors of subclinical seizures during scalp video-EEG monitoring in patients with epilepsy,” *International Journal of Neuroscience*, vol. 127, pp. 651–658, Aug. 2017.
- [18] S. Sunderam, I. Osorio, and M. G. Frei, “Epileptic seizures are temporally interdependent under certain conditions,” *Epilepsy Research*, vol. 76, pp. 77–84, Sept. 2007.
- [19] B. Oken and K. Chiappa, “Short-term variability in EEG frequency analysis,” *Electroencephalography and Clinical Neurophysiology*, vol. 69, pp. 191–198, Mar. 1988.

- [20] C. Geier, K. Lehnertz, and S. Bialonski, “Time-dependent degree-degree correlations in epileptic brain networks: from assortative to dissortative mixing,” *Frontiers in Human Neuroscience*, vol. 9, p. 462, 2015.
- [21] C. Geier and K. Lehnertz, “Long-term variability of importance of brain regions in evolving epileptic brain networks,” *Chaos: An Interdisciplinary Journal of Nonlinear Science*, vol. 27, p. 043112, Apr. 2017.
- [22] G. D. Mitsis, M. N. Anastasiadou, M. Christodoulakis, E. S. Papathanasiou, S. S. Papacostas, and A. Hadjipapas, “Functional brain networks of patients with epilepsy exhibit pronounced multiscale periodicities, which correlate with seizure onset,” *Human Brain Mapping*, vol. 41, no. 8, pp. 2059–2076, 2020.
- [23] S. V. Gliske, Z. T. Irwin, C. Chestek, G. L. Hegeman, B. Brinkmann, O. Sagher, H. J. L. Garton, G. A. Worrell, and W. C. Stacey, “Variability in the location of high frequency oscillations during prolonged intracranial EEG recordings,” *Nature Communications*, vol. 9, p. 2155, Dec. 2018.
- [24] P. J. Karoly, D. R. Freestone, R. Boston, D. B. Grayden, D. Himes, K. Leyde, U. Seneviratne, S. Berkovic, T. O’Brien, and M. J. Cook, “Interictal spikes and epileptic seizures: their relationship and underlying rhythmicity,” *Brain*, vol. 139, pp. 1066–1078, Apr. 2016.
- [25] E. C. Conrad, S. B. Tomlinson, J. N. Wong, K. F. Oechsel, R. T. Shinohara, B. Litt, K. A. Davis, and E. D. Marsh, “Spatial distribution of interictal spikes fluctuates over time and localizes seizure onset,” *Brain*, vol. 143, pp. 554–569, Feb. 2020.
- [26] M. O. Baud, J. K. Kleen, E. A. Mirro, J. C. Andrechak, D. King-Stephens, E. F. Chang, and V. R. Rao, “Multi-day rhythms modulate seizure risk in epilepsy,” *Nature Communications*, vol. 9, p. 88, Jan. 2018.
- [27] Z. Chen, D. B. Grayden, A. N. Burkitt, U. Seneviratne, W. J. D’Souza, C. French, P. J. Karoly, K. Dell, K. Leyde, M. J. Cook, and M. I. Maturana, “Spatiotemporal Patterns of High-Frequency Activity (80-170 Hz) in Long-term Intracranial EEG,” *Neurology*, Dec. 2020.
- [28] A. Burrello, L. Cavigelli, K. Schindler, L. Benini, and A. Rahimi, “Laelaps: An Energy-Efficient Seizure Detection Algorithm from Long-term Human iEEG Recordings without False Alarms,” in *2019 Design, Automation & Test in Europe Conference & Exhibition (DATE)*, pp. 752–757, Mar. 2019.
- [29] D. D. Lee and H. S. Seung, “Learning the parts of objects by non-negative matrix factorization,” *Nature*, vol. 401, pp. 788–791, Oct. 1999.
- [30] S. M. Atif, S. Qazi, and N. Gillis, “Improved SVD-based initialization for nonnegative matrix factorization using low-rank correction,” *Pattern Recognition Letters*, vol. 122, pp. 53–59, May 2019.
- [31] N. E. Huang, Z. Shen, S. R. Long, M. C. Wu, H. H. Shih, Q. Zheng, N.-C. Yen, C. C. Tung, and H. H. Liu, “The empirical mode decomposition and the Hilbert spectrum for nonlinear and non-stationary time series analysis,” *Proceedings of the Royal Society of London. Series A: Mathematical, Physical and Engineering Sciences*, vol. 454, pp. 903–995, Mar. 1998.

[32] N. E. Huang, M.-L. C. Wu, S. R. Long, S. S. P. Shen, W. Qu, P. Gloersen, and K. L. Fan, “A Confidence Limit for the Empirical Mode Decomposition and Hilbert Spectral Analysis,” *Proceedings: Mathematical, Physical and Engineering Sciences*, vol. 459, no. 2037, pp. 2317–2345, 2003.

[33] A. Y. Kaplan, A. A. Fingelkurts, A. A. Fingelkurts, S. V. Borisov, and B. S. Darkhovsky, “Nonstationary nature of the brain activity as revealed by EEG/MEG: Methodological, practical and conceptual challenges,” *Signal Processing*, vol. 85, pp. 2190–2212, Nov. 2005.

[34] A. A. Fingelkurts and A. A. Fingelkurts, “Operational Architectonics of the Human Brain Biopotential Field: Towards Solving the Mind-Brain Problem,” *Brain and Mind*, vol. 2, pp. 261–296, Dec. 2001.

[35] N. Rehman and D. P. Mandic, “Multivariate empirical mode decomposition,” *Proceedings of the Royal Society A: Mathematical, Physical and Engineering Sciences*, vol. 466, pp. 1291–1302, May 2010.

[36] N. E. Huang, *Hilbert-Huang Transform and Its Applications*. World Scientific, 2014.

[37] Y. Lv, R. Yuan, and G. Song, “Multivariate empirical mode decomposition and its application to fault diagnosis of rolling bearing,” *Mechanical Systems and Signal Processing*, vol. 81, pp. 219–234, Dec. 2016.

[38] N. Hurley and S. Rickard, “Comparing Measures of Sparsity,” *IEEE Transactions on Information Theory*, vol. 55, pp. 4723–4741, Oct. 2009.

[39] R. Tibshirani, “Regression Shrinkage and Selection via the Lasso,” *Journal of the Royal Statistical Society. Series B (Methodological)*, vol. 58, no. 1, pp. 267–288, 1996.

[40] Z. Wu and N. E. Huang, “A study of the characteristics of white noise using the empirical mode decomposition method,” *Proceedings of the Royal Society of London. Series A: Mathematical, Physical and Engineering Sciences*, vol. 460, pp. 1597–1611, June 2004.

[41] P. Flandrin, G. Rilling, and P. Goncalves, “Empirical mode decomposition as a filter bank,” *IEEE Signal Processing Letters*, vol. 11, pp. 112–114, Feb. 2004.

[42] N. ur Rehman and D. P. Mandic, “Filter Bank Property of Multivariate Empirical Mode Decomposition,” *IEEE Transactions on Signal Processing*, vol. 59, pp. 2421–2426, May 2011.

[43] H. Scheich, “Interval histograms and periodic diurnal changes of human alpha rhythms,” *Electroencephalography and Clinical Neurophysiology*, vol. 26, p. 442, Apr. 1969.

[44] D. C. Spencer, F. T. Sun, S. N. Brown, B. C. Jobst, N. B. Fountain, V. S. S. Wong, E. A. Mirro, and M. Quigg, “Circadian and ultradian patterns of epileptiform discharges differ by seizure-onset location during long-term ambulatory intracranial monitoring,” *Epilepsia*, vol. 57, pp. 1495–1502, Sept. 2016.

[45] M. K. Smyk and G. van Luijtelaar, “Circadian Rhythms and Epilepsy: A Suitable Case for Absence Epilepsy,” *Frontiers in Neurology*, vol. 11, 2020.

[46] D. Aeschbach, J. R. Matthews, T. T. Postolache, M. A. Jackson, H. A. Giesen, and T. A. Wehr, "Two circadian rhythms in the human electroencephalogram during wakefulness," *American Journal of Physiology-Regulatory, Integrative and Comparative Physiology*, vol. 277, pp. R1771–R1779, Dec. 1999.

[47] L. Cummings, A. Dane, J. Rhodes, P. Lynch, and A. M. Hughes, "Diurnal variation in the quantitative EEG in healthy adult volunteers," *British Journal of Clinical Pharmacology*, vol. 50, pp. 21–26, July 2000.

[48] D. A. Kaiser, "Ultradian and Circadian Effects in Electroencephalography Activity," *Biofeedback*, vol. 36, no. 4, p. 148, 2008.

[49] F. Chapotot, C. Jouny, A. Muzet, A. Buguet, and G. Brandenberger, "High frequency waking EEG: reflection of a slow ultradian rhythm in daytime arousal," *NeuroReport*, vol. 11, pp. 2223–2227, July 2000.

[50] M. I. Maturana, C. Meisel, K. Dell, P. J. Karoly, W. D'Souza, D. B. Grayden, A. N. Burkitt, P. Jiruska, J. Kudlacek, J. Hlinka, M. J. Cook, L. Kuhlmann, and D. R. Freestone, "Critical slowing down as a biomarker for seizure susceptibility," *Nature Communications*, vol. 11, May 2020.

[51] M. A. Kramer, W. Truccolo, U. T. Eden, K. Q. Lepage, L. R. Hochberg, E. N. Eskandar, J. R. Madsen, J. W. Lee, A. Maheshwari, E. Halgren, C. J. Chu, and S. S. Cash, "Human seizures self-terminate across spatial scales via a critical transition," *Proceedings of the National Academy of Sciences*, vol. 109, pp. 21116–21121, Dec. 2012.

[52] S. Arzy, G. Allali, D. Brunet, C. M. Michel, P. W. Kaplan, and M. Seeck, "Antiepileptic drugs modify power of high EEG frequencies and their neural generators," *European Journal of Neurology*, vol. 17, pp. 1308–1312, Oct. 2010.

[53] P. J. Karoly, H. Ung, D. B. Grayden, L. Kuhlmann, K. Leyde, M. J. Cook, and D. R. Freestone, "The circadian profile of epilepsy improves seizure forecasting," *Brain*, vol. 140, pp. 2169–2182, Aug. 2017.

[54] P. J. Karoly, D. M. Goldenholz, D. R. Freestone, R. E. Moss, D. B. Grayden, W. H. Theodore, and M. J. Cook, "Circadian and circaseptan rhythms in human epilepsy: a retrospective cohort study," *The Lancet Neurology*, vol. 17, pp. 977–985, Nov. 2018.

[55] F. Rakers, M. Walther, R. Schiffner, S. Rupprecht, M. Rasche, M. Kockler, O. W. Witte, P. Schlattmann, and M. Schwab, "Weather as a risk factor for epileptic seizures: A case-crossover study," *Epilepsia*, vol. 58, no. 7, pp. 1287–1295, 2017.

[56] R. R. van Koert, P. R. Bauer, I. Schuitema, J. W. Sander, and G. H. Visser, "Caffeine and seizures: A systematic review and quantitative analysis," *Epilepsy & Behavior: E&B*, vol. 80, pp. 37–47, 2018.

[57] E. Baldin, W. A. Hauser, A. Pack, and D. C. Hesdorffer, "Stress is associated with an increased risk of recurrent seizures in adults," *Epilepsia*, vol. 58, no. 6, pp. 1037–1046, 2017.

[58] C. W. Bazil and T. S. Walczak, "Effects of Sleep and Sleep Stage on Epileptic and Nonepileptic Seizures," *Epilepsia*, vol. 38, no. 1, pp. 56–62, 1997.

- [59] O.-Y. Kwon, H. S. Ahn, and H. J. Kim, “Fatigue in epilepsy: A systematic review and meta-analysis,” *Seizure*, vol. 45, pp. 151–159, Feb. 2017.
- [60] J. Bauer, “Interactions Between Hormones and Epilepsy in Female Patients,” *Epilepsia*, vol. 42, no. s3, pp. 20–22, 2001.
- [61] E. Taubøll, L. Sveberg, and S. Svalheim, “Interactions between hormones and epilepsy,” *Seizure*, vol. 28, pp. 3–11, May 2015.
- [62] S. Khan, L. Nobili, R. Khatami, T. Loddenkemper, C. Cajochen, D.-J. Dijk, and S. H. Eriksson, “Circadian rhythm and epilepsy,” *The Lancet Neurology*, vol. 17, pp. 1098–1108, Dec. 2018.
- [63] D. R. Freestone, P. J. Karoly, and M. J. Cook, “A forward-looking review of seizure prediction,” *Current Opinion in Neurology*, vol. 30, pp. 167–173, Apr. 2017.
- [64] R. A. B. Badawy, D. R. Freestone, A. Lai, and M. J. Cook, “Epilepsy: Ever-changing states of cortical excitability,” *Neuroscience*, vol. 222, pp. 89–99, Oct. 2012.
- [65] D. E. Payne, K. L. Dell, P. J. Karoly, V. Kremen, V. Gerla, L. Kuhlmann, G. A. Worrell, M. J. Cook, D. B. Grayden, and D. R. Freestone, “Identifying seizure risk factors: A comparison of sleep, weather, and temporal features using a Bayesian forecast,” *Epilepsia*, vol. 62, no. 2, pp. 371–382.